Volume 589, Issue 2 May 1, 2008 ISSN 0168-9002

ELSEVIER

NUCLEAR INSTRUMENTS & METHODS IN PHYSICS RESEARCH

Section A: accelerators, spectrometers, detectors and associated equipment

Editors:
William Barletta
(*Coordinating Editor*)
Robert Klanner
Fulvio Parmigiani
Fabio Sauli
David Wehe

Founding Editor – Kai Siegbahn

http://www.elsevier.com/locate/NIMA

Available online at www.sciencedirect.com
ScienceDirect

Nuclear Instruments and Methods in Physics Research A 589 (2008) 338–344

NUCLEAR INSTRUMENTS & METHODS IN PHYSICS RESEARCH Section A

www.elsevier.com/locate/nima

An axis of rotation alignment system for high-resolution pinhole SPECT imaging

Joong Hyun Kim[a,b,e], Jae Sung Lee[a,b,d,e,*], Min Jae Park[a,c], Won Woo Lee[a], Soo Mee Kim[a,b], Yu Kyeong Kim[a], Sang Eun Kim[a,e], Dong Soo Lee[a,b,e]

[a]Department of Nuclear Medicine, Seoul National University, 28 Yungun-Dong, Chongno-Gu, Seoul 110-744, Republic of Korea
[b]Interdisciplinary Program in Radiation Applied Life Science Major, Seoul National University, Seoul 110-744, Republic of Korea
[c]Department of Biomedical Engineering, Seoul National University, Seoul 110-744, Republic of Korea
[d]Department of Biomedical Sciences, College of Medicine, Seoul National University, Seoul 110-744, Republic of Korea
[e]Institute of Radiation Medicine, Medical Research Center, Seoul National University, Seoul 110-744, Republic of Korea

Received 7 November 2007; received in revised form 17 January 2008; accepted 1 February 2008
Available online 26 February 2008

Abstract

We developed a simple geometric calibration method for modified animal pinhole single photon emission computed tomography (SPECT) imaging systems using a laser alignment system that does not require additional calibration scans, and verified the feasibility of this system. An optical system consisting of a laser generator and a reflecting mirror, and an alignment method using this system were developed. After laser alignment had been completed, SPECT scans of a Tc-99m line source were performed. After acquiring data with complete alignment, the rotation stage was moved along the y-axis (parallel to the detector plane) to acquire off-axis data. Using these on- and off-axis settings, a micro-performance phantom with hot-rod inserts was scanned after filling with Tc-99m solution. Reconstructed images of the line source and the hot-rod phantom showed that image degradation was minimized when the rotation center was completely aligned using our system. The spatial resolution of the reconstructed image measured using the line source was finest under complete alignment. Under this condition, the smallest hot rod (1.2 mm diameter) was resolved in the SPECT image acquired using a 0.5 mm pinhole aperture. The effects of misalignment were clearly observable in off-axis images; only hot rods with more than 3.2 mm diameter were resolved in 1 mm off-axis image whereas there were no resolvable hot rods with more than 2 mm off-axis image. This system of which the feasibility was verified in the present study will be useful for low-cost molecular imaging studies using single photon emitting tracers.

PACS: 87.57.uh; 87.57.U−; 29.40.Mc; 42.30.Va

Keyword: SPECT; Molecular imaging; Center of rotation error; Pinhole collimator

1. Introduction

Single photon emission computed tomography (SPECT) imaging with a pinhole collimator is a powerful molecular imaging research tool because it provides information on the spatial and temporal distributions of single photon emitting molecular imaging probes at a spatial resolution that is high enough for small animal (usually rodents) studies [1–5].

It is also possible to improve photon collection efficiency (sensitivity) using multiple gamma-ray detectors and pinhole apertures [4,6–8]. Although the merits of these multi-pinhole SPECT imaging methods are evident, it should also be noted that expensive dedicated animal SPECT systems, or alternatively, multi-pinhole collimators are required for this advanced imaging technique. Therefore, modified animal SPECT imaging systems based on a clinical gamma camera and smaller pinhole apertures than

*Corresponding author at: Department of Nuclear Medicine and Biomedical Sciences, Seoul National University College of Medicine, 28 Yungun-Dong, Chongno-Gu, Seoul 110-744, Republic of Korea.
Tel.: +82 2 2072 2938; fax: +82 2 745 2938.
E-mail address: jaes@snu.ac.kr (J.S. Lee).

0168-9002/$ - see front matter © 2008 Elsevier B.V. All rights reserved.
doi:10.1016/j.nima.2008.02.033

those used clinically are still regarded as a practical alternative to dedicated imaging units [4,8–10].

One of the obstacles concerning the use of clinical gamma camera systems for this purpose is that usually only one pinhole collimator is available, because the pinhole collimator is commonly used for unidirectional planar imaging of the thyroid or skeletal joints, but pinhole SPECT is rarely performed in the clinical environment. The rotation of a single detector or unbalanced multiple detectors, due to the availability of only one pinhole collimator, results in serious angle-dependent fluctuations in the distance of the detector from the center because of the gravitational effect of the mass of the detector and the collimator [5,8,11,16].

Thus, the rotation of objects in front of the fixed detector head might provide a practical solution in such situations reducing the so-called 'center of rotation (COR) error'. In the strategy of rotating object, however, misalignment between the ideal axis of rotation and the center of the rotating stage (Fig. 1) can cause another type of COR error [10,12–14]. The effect of this misalignment is illustrated using mathematical phantom data in Fig. 2. After an intentional shift of the center of rotation, three point sources were projected for each rotation angle to generate a sinogram. In the sinogram, we can identify offsets in the trajectories of the point sources from the center over all the projection angles (Fig. 2A). A reconstructed image of this sinogram shows significant distortion of the object: the points are reconstructed as donuts in Fig. 2B.

In this study, we developed a laser alignment system that provides a convenient and efficient solution for misalignment errors, and we tested the feasibility of this system using a line source and cylindrical phantom data.

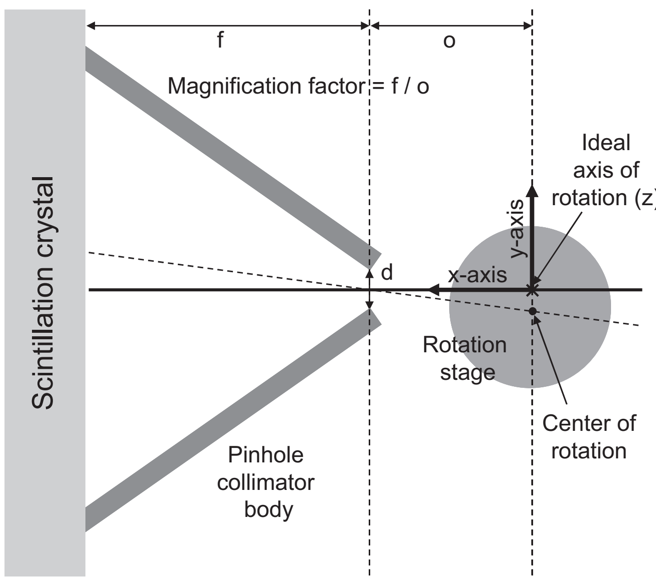

Fig. 1. Geometry of pinhole SPECT imaging with a stationary camera and a rotating object.

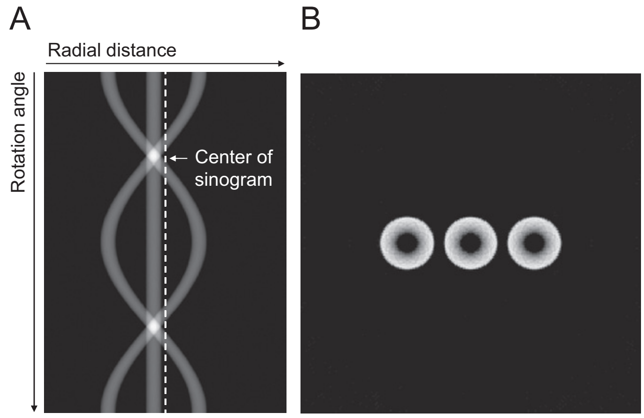

Fig. 2. Effects of positioning errors due to mismatches between the ideal axis of rotation and the center of rotation: (A) simulated sinogram of three point sources with such a mismatch, (B) reconstructed image of the point sources.

Table 1
Specifications of the Phillips Skylight SPECT system

Description	Type or dimenxsion
Non-Anger digital detector	1 ADC/PMT
Field of view	38.1 cm × 50.8 cm (15″ × 20″)
Crystal material	NaI(Tl)
Crystal thickness	9.5 mm (3/8″)
Photomultiplier tubes/head	55

2. Materials and methods

2.1. SPECT system with a pinhole collimator

For the pinhole SPECT studies, a Skylight dual-head SPECT system (Phillips Medical System, Cleveland, OH, USA) was used. The specification of this system is shown in Table 1. The detector head of this system was equipped with a pinhole collimator. Although the size of the full field-of-view (FOV) was 381 cm × 50.8 cm (15″ × 20″), only a central FOV of 25.4 cm × 25.4 cm (10″ × 10″) was used for pinhole imaging because of the restricted collimator geometry.

The pinhole collimator consists of a main body and a replaceable aperture (Fig. 3). Pinhole apertures provided by the manufacturer for the clinical purposes have hole diameters of >3.0 mm to achieve sufficient system sensitivity. However, the spatial resolutions possible at these apertures are not suitable for small-animal imaging. Thus we manufactured pinhole apertures with smaller hole diameters of 0.5, 1.0 and 2.0 mm to improve the spatial resolution (Precise Corporation, Caryville, TN, USA). The distance from the pinhole to the crystal surface was 17.8 cm (7″) and the cone angle of the pinhole main body was 70°.

2.2. Object rotation stage and laser alignment system

A rotation stage driven by a step motor and computer control program (to control the rotation angle and time

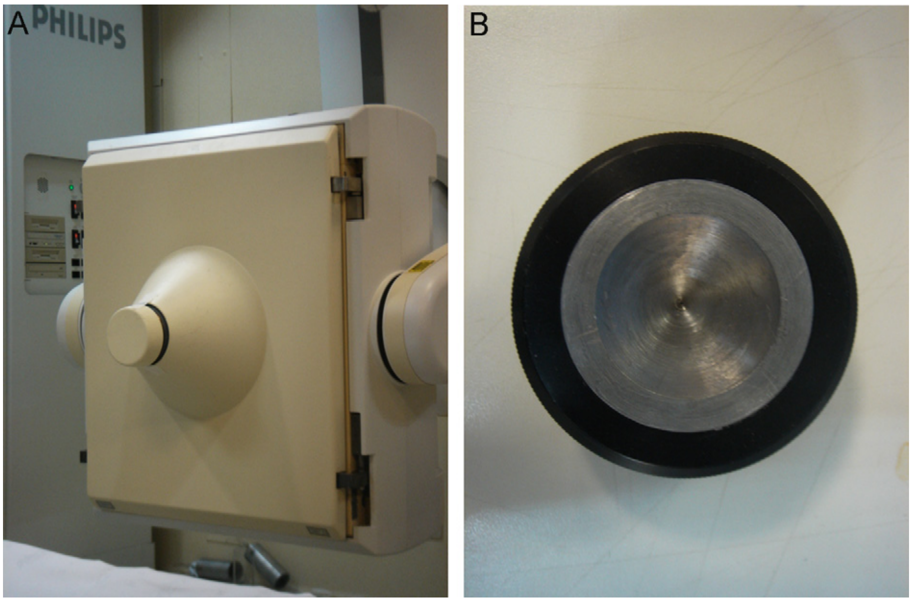

Fig. 3. Pinhole collimator: (A) main body attached on the detector, (B) aperture of 0.5 mm diameter.

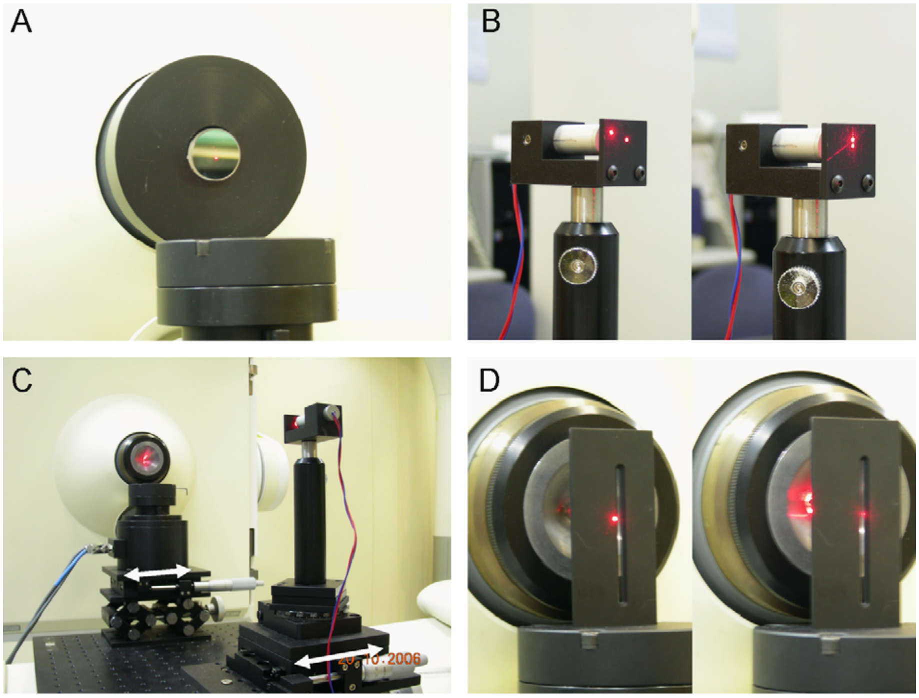

Fig. 4. Laser alignment system and rotation stage: alignment was performed through steps (A–D).

interval of the step motor) was developed. The step motor was connected to a PC using a PCI-8132 control card (Nam Il Optical Components Corp., Incheon, Korea).

Fig. 4 shows the laser alignment system that we developed and explains the alignment procedure step by step. Laser light was generated and reflected by a mirror positioned in front of the pinhole aperture and in parallel to the detector plane (Fig. 4A). If the reflected laser beam hits the point beam origin, the direction of the laser beam was regarded as being perpendicular to the detector plane (Fig. 4B). The direction of the laser beam was controlled by a precise manual rotation controller. If the laser beam did not go into the pinhole after the mirror had been removed, the laser generator was translated in two directions (y, z) parallel to the detector plane until the beam reached the pinhole (Fig. 4C). Agreement between the laser beam line and the axis that is normal to the detector plane and passing the pinhole can be achieved using the above procedures. Finally, the step motor was translated so that the laser beam line intersected the COR using a slit positioned precisely at the rotation center (Fig. 4D). Neither the laser nor the detector was moved in this step.

3. Experiments

After laser alignment had been completed, as described above, a SPECT scan of a Tc-99m line source (inner diameter = 0.5 mm, activity = 740 kBq) was performed using a 0.5 mm pinhole aperture. The line source was placed along the axis of the scanner (z-axis) in a standing position and was fixed to the center of the rotation stage. The distance between the pinhole and line source was 5 cm (magnification factor = 17.8/5.0 = 3.56). After acquiring data under complete alignment, the rotation stage was moved along the y-axis (parallel to the detector plane) in steps of 0.1 mm from 0 to 0.6 mm, and in steps of 0.2 mm from 0.6 to 1.0 mm to acquire off-axis data. For each SPECT scan, 120 projections were acquired in the step-and-shoot mode over a total of 30 min (15 s/projection) for full angle (360°). The energy window was set at 140.5 keV with a 15% width. Images were reconstructed as $128 \times 128 \times 128$ (voxel size = 0.1 mm) matrices using a filtered back projection algorithm with the Ramp filter. For quantitative comparisons, profiles were drawn on the average images of the middle eight transaxial slices to pass the maximum pixels. Full-width at half-maximum (FWHM) values were then determined by linear interpolation between adjacent pixels at half of the profile peak, which was determined by parabolic fitting using peak point and two adjacent peaks [15].

Using similar on- and off-axis settings, a micro-performance phantom with hot-rod inserts (Data Spectrum Corp., NC, USA, Fig. 5) was scanned after filling it with Tc-99m solution (555 MBq). The SPECT scan protocol was the same as that used for line source imaging. The distance from the pinhole to the center of the step motor was 5.7 cm (magnification factor = 3.12). Using a 0.5 mm pinhole aperture, on- and various off-axis (1.0–5.0 mm offset in steps of 1.0 mm) scans were performed. For comparison purposes, on-axis scans with various pinhole aperture diameters (1.0, 2.0 and 3.0 mm) were also acquired. A Hanning filter with a cut-off frequency of 0.45 cycle/pixel was used for filtered back projection reconstruction. Image qualities of the reconstructed images were assessed and the size of the smallest hot-rod insert resolved was measured. The effects of off-axis rotation and pinhole aperture size on image degradation were then compared.

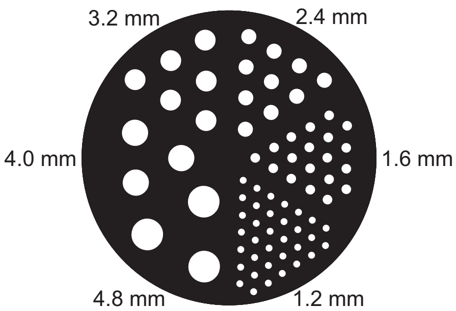

Fig. 5. Cross-section of micro performance phantom insert (Data Spectrum). The diameter of insert is 43 mm, and diameters of hollow channels are 1.2, 1.6, 2.4, 3.2, 4.0 and 4.8 mm. The hollows are separated by two times the diameter.

4. Results

On the projection images of the line source acquired in the on-axis condition, profiles perpendicular to the line source were drawn and peak positions on the profiles were determined. The peak position of the profile for each projection angle is shown in Fig. 6. The y-axis represented by 'pixel' is unitless since it could be obtained by dividing the distance (mm) between the peak position of the profile and the center of the projection image by pixel size (mm). Almost no variation was observed in the position of the peak located precisely at the center of the projection image. The physical size of a pixel was 1.07 mm in detector space (distance between the ticks in the y-axis of Fig. 6) and the variation of the peak position was not higher than the pixel size.

Line profile during on-axis condition and reconstructed images of the line source during on-axis and various off-axis conditions are shown in Fig. 7A and B. The middle eight transaxial slices (total thickness = 0.8 mm) were averaged to improve image quality. As the offset between the rotation center and the axis of rotation increased, the intensity of the cross-section of line source became more dispersed; at an offset of >0.8 mm, the cross-section of the line source appeared doughnut-like rather than as a point. The FWHM values of the profile across maximum cross-section intensities are plotted against offset values in Fig. 7C. The figure shows that minimal degradation of the image was achieved with complete rotation center alignment (offset = 0 mm) using our system.

Fig. 8 also shows the feasibility of our system. When completely aligned, the smallest hot rod (1.2 mm diameter) was resolved in the SPECT image acquired with the 0.5 mm

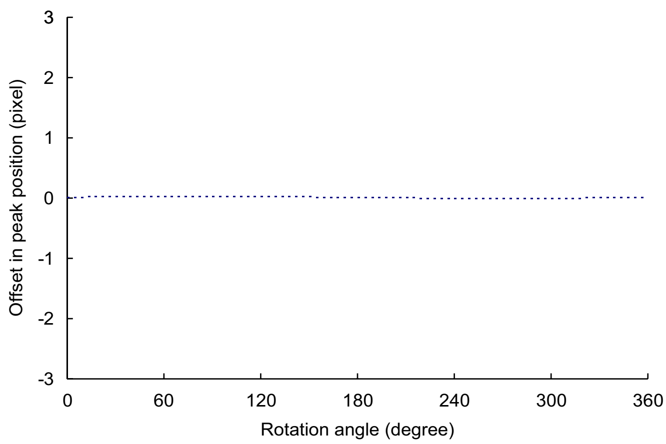

Fig. 6. Peak positions of profiles at each projection angle (offset from the center of projection images in unit of pixel). The variation of the peak position was less than the size of a pixel.

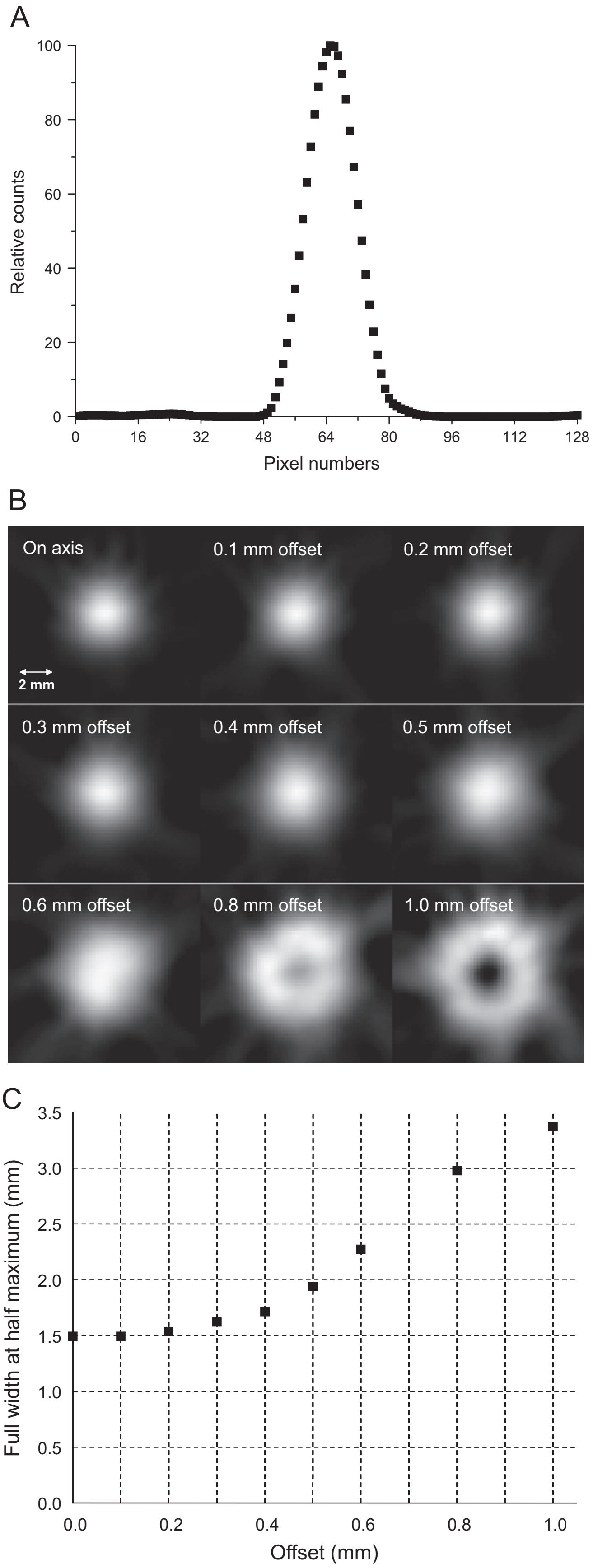

pinhole aperture (Fig. 8A). The effects of misalignment were clearly observable in off-axis images: only hot rods of more than 3.2 mm diameter were resolved in 1 mm off-axis images and no hot rods were resolved at an offset of more than 2 mm off-axis. Severe distortion appeared in off-axis images at large offsets: the imaginary patterns of cold hollows were observed in reconstructed images (Fig. 8A).

However, image degradation due to aperture size (Fig. 8B) was less severe than that caused by misalignment in terms of lesion detectability. We were able to identify the smallest hot rod using pinhole apertures of 0.5 and 1.0 mm, and rods of more than 1.6 and 2.4 mm were resolved using pinhole apertures of 2.0 and 3.0 mm, respectively.

5. Discussion

Most clinical imaging devices are unsuitable for imaging of small animals because of their inadequate spatial resolution relative to the size of animals. In this respect, SPECT is exceptional because high-resolution imaging is possible using a clinical gamma camera or SPECT system if they are equipped with pinhole apertures with a micro diameter. Large magnification of projection is possible by altering pinhole geometry and blurring of a source can be reduced using small apertures.

To scan animals using the micro-pinhole SPECT system, two different acquisition methods are used. The first one is rotating the gamma camera around animals, as is performed in clinical studies. This method has an advantage of being comfortable for animals and is most suitable for multi-head SPECT systems, in which all detectors are equipped with identical pinhole collimators. However, the careful calibration of angle-dependent positional errors is mandatory, due to the heavy mass of detectors and collimators, if good image qualities are to be acquired using this method [8,11,16].

The other method is rotating the object (usually in a standing position) in front of a stationary pinhole camera(s). This method would be the better choice if rotation of the camera is not possible or if mass imbalance between detectors causes severe COR error. The only calibration procedure necessary is precise alignment between the COR and the ideal axis of rotation, if influence of mechanical and electronic shift (MES) of the collimator are negligible. In fact, MES is another possible source of positioning error in addition to the mismatch between the rotation center and the ideal axis (Axis of Rotation Mismatch: ARM) in the stationary pinhole camera. Although the ARM can be adjusted using our alignment system, it does not allow for the correction of MES.

Fig. 7. Results of line source imaging in the on-axis and various off-axis conditions using a 0.5-mm pinhole aperture: (A) a line profile across the line source during on-axis condition, (B) transaxial slices of reconstructed images, (C) FWHM values of the profiles across the maximum intensity of cross-sections plotted against offset values.

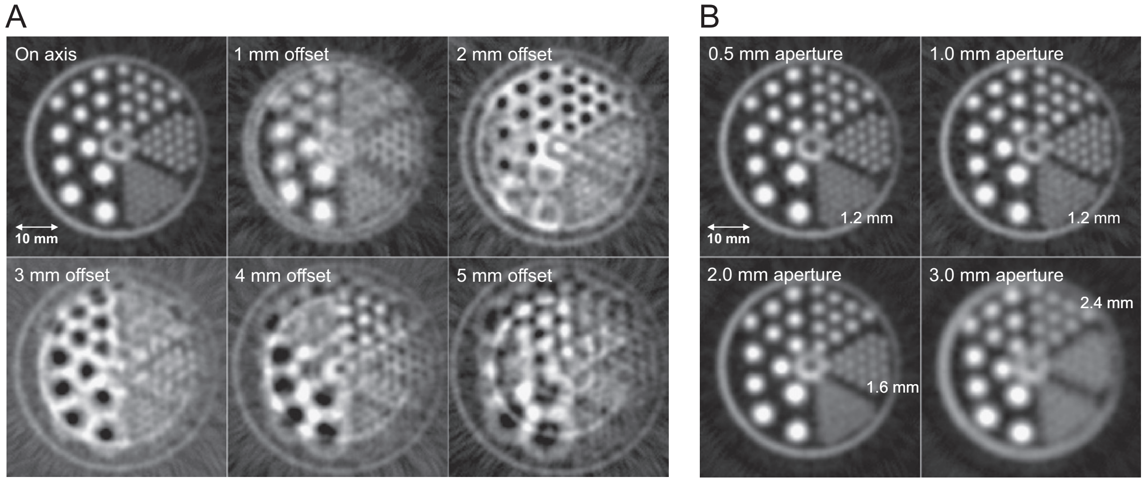

Fig. 8. Results of phantom imaging: (A) transaxial slices of reconstructed images acquired in the on-axis and various off-axis conditions using a 0.5-mm pinhole aperture, (B) images acquired in the on-axis condition using various pinhole aperture diameters.

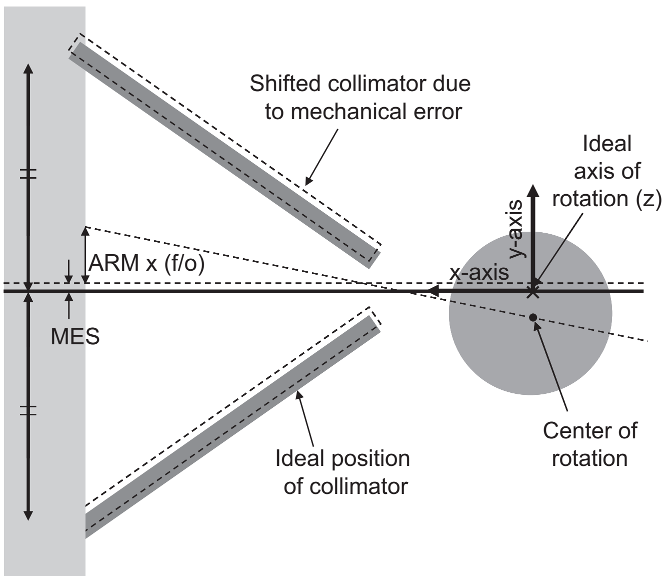

Fig. 9. Main components contributing to pinhole SPECT positioning errors. The mechanical and electrical shift (MES) error is relatively smaller than the axis of rotation mismatch (ARM) because the ARM in image space is scaled up by magnification factor (*f*/*o*).

However, the degradation of spatial resolution due to MES would not be significant because its effects can be scaled down by the pinhole magnification of objects, as shown in Fig. 9 and described by the following equation:

Positioning error in object pace

$$= \{\mathrm{ARM}(f/o) + \mathrm{MES}\}/(f/o) = \mathrm{ARM} + \mathrm{MES}/(f/o)$$

where f/o is the magnification factor of the pinhole collimator (Fig. 1).

MES in our pinhole camera was less than 1 mm when we measured it several times using a line source during our experiments, and the magnification factor was 3–4. Thus, the positioning error due to MES was approximately 0.3 mm, which is much smaller than the spatial resolution of the system.

To compensate for ARM error in pinhole SPECT imaging with a stationary camera and a rotating object, Wu et al. [10] scanned a line source that was coaxial with the rotating stage prior to SPECT imaging of objects and projection data were shifted by the distance between the line source and center of the image matrix. When we used this method before developing our system, we found it impractical for us because, to perform this procedure, much time was needed to prepare the line source and acquire sufficient photon counts to allow calibration, mainly because of the small volume and low activity of the line source.

Another approach 'the auto-calibration method' was suggested by DiFilippo and Riffe, in which ^{57}Coor ^{153}Gd point sources attached on the animal holder were scanned simultaneously after injecting animals with Tc-99m [17]. Their activity distributions were separated using different energy windows for detected photons. Reliable correction was possible even for low activity of point sources and positioning errors were of the order of 0.1 mm. However, crosstalk or contamination of emission data by 136 keV photons from the ^{57}Copoint source can cause a source of misinterpretation of study results [18,19]. In addition, the calibration sources cannot be used universally for SPECT imaging studies with other radioisotopes, because they have different photon energies from the Tc-99m.

Using the laser alignment system developed in this study, neither additional scanning of the calibration source nor post-processing of projection data was required. Moreover, only a small amount of extra time is required to achieve alignment during the experimental setup process. The results of our experiments using the line source and a hot-rod phantom show the usefulness of our devised system in terms of minimizing the axis of rotation mismatch (ARM) errors, and demonstrate the importance of ARM correction to obtain highly accurate pinhole SPECT images

(Figs. 7 and 8). Even small ARM errors can result in almost useless images (Fig. 8A). Moreover, performance degradations in terms of lesion detection due to ARM errors were much more severe than those caused by image blurring due to the use of large pinhole apertures.

6. Conclusion

For high-resolution pinhole SPECT imaging using a clinical gamma camera system, we developed an optical alignment method that minimizes positioning errors due to a mismatch between the ideal axis of rotation and the rotating center. This system of which the feasibility was verified in the present study will be useful for low-cost molecular imaging studies using single photon emitting tracers.

Acknowledgments

This work was supported by Grants from the Basic Research Program of the Korean Science & Engineering Foundation (R01-2006–000–10296–0) and the Basic Atomic Energy Research Institute Program (M20508050002–05B0805–00210, 2007–01022) funded by the Ministry of Science and Technology, Korea and Seoul R&BD Program (1 0 5 5 0) funded by the Seoul Development Institute. The authors wish to thank Dr. Ling Shao at Philips Medical Systems and Mr. David York at Precise Corp. for their help during the manufacture of micro-apertures and Dr. Yong Choi and Dr. Tae Yong Song at the Samsung Medical Center, Sungkyunkwan University and Mr. Seong Ho Kim at Seoul National University Hospital for their support during the development of the rotating stage.

References

[1] M.G. Pomper, J.S. Lee, Curr. Pharm. Des. 11 (2005) 3247.
[2] Y. Seo, D.W. Gao, B.H. Hasegawa, M.W. Dae, B.L. Franc, Med. Phys. 34 (2007) 1217.
[3] P.D. Acton, S.R. Choi, K. Plössl, H.F. Kung, Eur. J. Nucl. Med. Mol. Imaging 29 (2002) 691.
[4] B. Vastenhouw, F.J. Beekman, J. Nucl. Med. 48 (2007) 487.
[5] C. Bai, L. Shao, J. Ye, M. Durbin, IEEE Trans Nucl. Sci. NS-50 (2003) 1528.
[6] M.C. Rentmeester, F. van der Have, F.J. Beekman, Phys. Med. Biol. 52 (2007) 2567.
[7] Z. Cao, F. Bal, R. Accorsi, P.D. Acton, Phys. Med. Biol. 50 (2005) 4609.
[8] S.D. Metzler, R.J. Jaszczak, N.H. Patil, S. Vemulapalli, G. Akabani, B.B. Chin, IEEE Trans. Med. Imaging 24 (2005) 853.
[9] J.B. Habraken, K. de Bruin, M. Shehata, J. Booij, R. Bennink, B.L. van Eck Smit, et al., J. Nucl. Med. 42 (2001) 1863.
[10] M.C. Wu, D.W. Gao, R.E. Sievers, R.J. Lee, B.H. Hasegawa, M.W. Dae, J. Am. Coll. Cardiol. 42 (2003) 576.
[11] S.D. Metzler, K.L. Greer, R.J. Jaszczak, IEEE Trans Med. Imaging 24 (2005) 361.
[12] D. Bequé, J. Nuyts, G. Bormans, P. Suetens, P. Dupont, IEEE Trans Med. Imaging 22 (2003) 599.
[13] M.C. Wu, B.H. Hasegawa, M.W. Dae, Med. Phys. 29 (2002) 2830.
[14] L.R. MacDonald, B.E. Patt, J.S. Iwanczyk, B.M.W. Tsui, Y. Wang, E.C. Frey, et al., IEEE Trans. Nucl. Sci. NS-48 (2001) 830.
[15] National Electrical Manufacturers Association. NEMA NU-1 Standard Publication NU-1-2001: performance measurements of scintillation cameras. Rosslyn, VA: National Electrical Manufacturers Association, 2001.
[16] S.D. Metzler, K.L. Greer, K. Bobkov, R.J. Jaszczak, IEEE Trans Nucl. Sci. NS-51 (2004) 603.
[17] F.P. Di Filippo, M.J. Riffe, IEEE Nucl. Sci. Symp. Conf. Rec. (2005) 1782.
[18] P. Hannequin, J. Mas, G. Germano, J. Nucl. Med. 41 (2000) 728.
[19] B.H. Brinkmann, M.K. O'Connor, T.J. O'Brien, B.P. Mullan, E.L. So, R.A. Robb, J. Nucl. Med. 40 (1999) 677.